***PREPRINT**: Journal of Wind Engineering and Industrial Aerodynamics 93(12): 905-928.*

High-resolution wind-driven rain measurements on a low-rise building – experimental data for model development and model validation

Bert Blocken* [(a)], Jan Carmeliet [(a,b)]

(a) Laboratory of Building Physics, Department of Civil Engineering, Katholieke Universiteit Leuven, Kasteelpark Arenberg 40, 3001 Leuven, Belgium
(b) Building Physics Group, Faculty of Building and Architecture, Technical University Eindhoven, P.O. box 513, 5600 MB Eindhoven, The Netherlands

Abstract

With the specific intention to provide experimental data for model development and model validation, a new measurement set-up for wind, rain and wind-driven rain (WDR) has been designed and installed at the Laboratory of Building Physics (Katholieke Universiteit Leuven). This paper focuses on the new measurement set-up and on the obtained measurement results. The CFD-based design and the installation of the measurement set-up are outlined and samples of the database containing the wind, rain and high-resolution WDR measurements are provided and discussed. This paper also provides the link to a website from which the experimental WDR database can be downloaded. Finally, the use of this data to determine WDR coefficients and their use in WDR assessment are briefly addressed.

Keywords: Wind-driven rain; Driving rain; Air flow; Raindrop; Building; Experimental database; Web file download; Validation; Numerical simulation; Coefficient; Guidelines

1. Introduction

Wind-driven rain (WDR) is an important boundary condition for the study of the hygrothermal performance and the durability of building facades and for their design. Three categories of methods for quantifying WDR on building facades exist: (1) measurements, (2) semi-empirical models and (3) numerical simulation models that are based on Computational Fluid Dynamics (CFD). A review of these methods is provided in [1].

Since the first WDR measurements on building facades were conducted in 1937 by Holmgren in Trondheim, Norway [1], measurements have been the primary tool in WDR studies. They not only provide a direct indication of the amount of WDR falling onto different parts of a building facade but they are also essential for the development and the validation of semi-empirical models and numerical simulation models. Especially the vast increase of the use of CFD in WDR studies in the past fifteen years [e.g. 1-10] and the subsequent need for CFD model validation have strengthened the need for adequate experimental WDR databases. Although a large amount of measurements have been performed in the past, a review of the literature has pointed out that only very few of these have been published in a form that can be suitable for model development and model validation. This is believed to be the most important reason for the fact that the validation of CFD modeling of WDR is still lacking. Adequate experimental data should comprise and/or be accompanied by the following information: (1) a detailed description of the building site and the building geometry; (2) a detailed description of the measurement set-up; (3) measurements of the reference wind speed, the reference wind direction and the horizontal rainfall intensity (i.e. the rainfall intensity through a horizontal plane) that have been conducted near the building site and in "free-field" conditions, i.e. at a position that is not significantly influenced by the presence of the building; (4) WDR measurements at the facade(s) with a high resolution in space and time

* Corresponding author: Bert Blocken, Laboratory of Building Physics, K.U.Leuven, Kasteelpark Arenberg 40, 3001 Leuven, Belgium. Tel.: +32 (0) 16-321345 - Fax: +32 (0) 16-321980
E-mail address: bert.blocken@bwk.kuleuven.be

and (5) error estimates for the WDR measurements. The latter aspect is very important as recent research has shown that WDR measurements can suffer from large measurement errors (up to 100%) [8,11,12].

This paper presents an experimental WDR database that satisfies the above-mentioned requirements. At the Laboratory of Building Physics (Katholieke Universiteit Leuven), a new measurement set-up for wind, rain and WDR has been designed and installed with the specific intention to provide experimental data for model development and model validation. The paper focuses on the new measurement set-up and on the obtained measurement results. In section 2, the CFD-based design and the installation of the measurement set-up are outlined. In section 3, samples of the database containing the wind, rain and the high-resolution WDR measurements are provided and the link to a website from which the experimental WDR database can be downloaded is made available. In section 4, the use of experimental data to determine WDR coefficients and their use in WDR assessment are briefly addressed.

2. Measurement set-up: design and installation

2.1. Building and building site

The full-scale building that was selected for the measurements is the VLIET-HAMTIE K20 test building [•]. This test building was designed and constructed by the Laboratory of Building Physics (Katholieke Universiteit Leuven) as a result of the 1993 VLIET programme of the Flemish Government. The VLIET building is situated in Heverlee, Leuven, at the K.U.Leuven University campus. Its construction was completed in October 1996 and it has been one of the major research instruments of the Laboratory of Building Physics since that time. Its principal goal is to investigate highly-insulated building-envelope parts exposed to the outside climate. To this end, the building is made up of a steel and concrete frame in which a large number of different test walls and test roofs can be built. The main research subjects are energy efficiency, hygrothermal behavior and durability. As WDR is one of the most important boundary conditions for the energy efficiency, the hygrothermal behavior and the durability of building facades, the building site, the location of the building on the site and the building design were specifically focused on WDR exposure. In Flanders, the direction of the prevailing winds is south-west. During rain, this is even more pronounced (Hens [13]). To obtain maximum exposure to WDR, the "most unsheltered" site in the neighborhood was selected, the building was located in the east corner of the site (as far as possible from the trees and other obstructions that are situated in the south-west direction) and it was designed as a long box with one of the longitudinal facades facing south-west.

The VLIET building consists of two main modules, the flat-roof module and the sloped-roof module (Fig. 1). In between the main modules, there is a small terrace module. The building is 25.2 m long and 7.2 m wide. The height of the flat-roof module and the sloped-roof module is 4.3 m and 7.9 m respectively. The terrace height is 3.95 m. Roof overhang varies along the length axis of the building as indicated in Fig. 1. A view of the terrain situated south-west of the test building is provided in Fig. 2. The elements providing shielding from wind in the direct vicinity of the building are some low agricultural constructions to the south (which are situated about 80 m in front of the south-west facade) and a row of high poplars to the west side. The trees are about 50 to 60 m high and they are positioned along a straight line. The row of trees is situated closest to the sloped-roof-module corner. The distance between this corner and the trees, measured in south-west direction, is about 70 m, while the distance between the middle of the south-west facade and the row of trees, measured in south-west direction, is about 130 m. Further away in south-west direction, concentrations of mainly low-rise buildings are located (not visible in Fig. 2). Figs. 3a-b illustrate the south-west facade of the VLIET building. Note that a number of test facades are protruded/recessed compared to the others.

At the time of the building completion in 1996, a (limited) set-up for WDR measurements was installed. This set-up has provided valuable data for early WDR studies. However, for validation studies it was necessary to design and install a new and improved measurement set-up. The improved measurement set-up was completed in the beginning of 2001. It consists of (1) a new meteorological mast positioned in front of the south-west facade that is equipped with three cup anemometers and one ultrasonic anemometer (Figs. 3d-e), (2) a capacitance rain gauge surrounded by a semi-circular turf wall (Fig. 3c) and (3) a large number of new WDR gauges (Fig. 1).

[•] VLIET = VLaams Impulsprogramma voor EnergieTechnologie (Flemish Impulse programme for Energy Technology); HAMTIE = Heat-Air-Moisture Transfer in highly Insulated building Envelope parts.

2.2. Wind

The old meteorological mast is positioned on the building roof and will therefore be situated in the wind-flow pattern that is disturbed by the building (Fig. 4). As a result it does not provide suitable reference wind-speed and wind-direction values. The intention of the new meteorological mast was to measure the vertical profile of the mean horizontal wind speed upstream of the south-west facade, outside the wind-flow pattern that is disturbed by the building (for south-west wind). Because of the complexity of the terrain in front of the south-west facade (low-rise buildings, trees: see Fig. 2), the position of the mast had to be chosen with care. The measured profile should be a representative input for numerical simulations. In the numerical simulations to be conducted around the VLIET building (for south-west wind), it is the intention not to include the complexity of the upstream terrain and to assume a homogeneous, equilibrium approach-flow wind-speed profile. Because in reality the site is definitely situated in an internal boundary layer (IBL) and the wind profile is not in equilibrium but developing over the site, the best representative wind-speed profile that can be taken is the profile as close as possible to the building. On the other hand, it was recognized that the building causes an important upstream disturbance of the wind-flow field and that the mast should be positioned outside this region. CFD simulations with the commercial code Fluent 5.4 (RANS, realizable k-ε model [14], standard wall functions [15]) of the 3D wind-flow pattern around the VLIET building have been used to determine the extent of the disturbed region in the upstream direction, for south-west wind direction. Based on these results, the mast (10 m high) was positioned at a distance of 20 m in front of the south-west facade, as indicated in Fig. 4. The results of the CFD analysis (mean wind-speed values) are given in Fig. 5. The simulations were conducted with a grid obtained by grid-sensitivity analysis (unstructured tetrahedral grid with 1,017,518 control volumes), by using a logarithmic wind-speed inflow profile ($y_0 = 0.03$ m) and a reference wind speed $U_{10} = 10$ m/s. The blockage ratio was 3.4%. Fig. 5d shows the axis conventions. Figs. 5a-b illustrate the vertical profiles of each mean wind-speed component (U: streamwise, V: vertical, W: lateral) and of the magnitude of the resultant horizontal wind-velocity vector ($Z = \sqrt{U^2 + W^2}$) at two positions: (1) Fig. 5a: at the position of the new meteorological mast (i.e. 20 m upstream of the south-west facade, see Fig. 5d) and (2) Fig. 5b: at the position of the old mast on top of the building (i.e. 3.6 m downstream of the south-west facade, see Fig. 5d). Comparing these figures, the following observations are made:

1. Fig. 5b. The old meteorological mast on top of the building is clearly situated in the disturbed wind-flow pattern. Although the approach flow has only a streamwise velocity component (U), the velocity vector at the top of the mast has important vertical (V) and lateral (W) components. Note that the wind speed labeled Z in the figure is the magnitude of the resultant horizontal vector.
2. Fig. 5a. At the position of the new meteorological mast, i.e. at a distance of 20 m south-west of the facade, the disturbance of the flow field is much less pronounced. The vertical and lateral components are small. The streamwise wind speed U and the resultant horizontal wind speed Z are practically the same.

Fig. 5c compares the resultant horizontal wind speed Z at varying distance from the south-west facade. The following observations are made:

1. As we approach the building, the Z-profiles are increasingly disturbed by the presence of the building (wind-blocking effect [10]; decrease of upstream wind speed).
2. The Z-profile at a distance of 20 m differs only slightly from the profile further upstream (40 m) (the difference is 2.5% at y = 10 m height).
3. The value of Z at the position of the cup anemometer on top of the old meteorological mast (distance – 3.6 m, measuring height 8.8 m) and the value at the position of the ultrasonic anemometer (new mast, distance 20 m, measuring height 10 m) appear to be practically the same (difference is 0.5%). It is noted that this is a lucky coincidence for south-west wind direction. For other wind directions, this will not be the case.

The new meteorological mast is equipped with three cup anemometers (at 2, 4 and 6 m height) and with an ultrasonic anemometer at 10 m (standard measuring height) (Fig. 3d-e and Fig. 4). The ultrasonic anemometer is more accurate than the cup anemometers. An often mentioned disadvantage of cup anemometers is the so-called cup overspeeding, which is a bias in the measured mean wind speed due to fluctuations in the longitudinal wind-speed component (turbulence). According to Kristensen [16], overspeeding only in extreme cases exceeds about 2%. However, Kristensen has shown that the fluctuations in the other wind-speed components give rise to other types of bias. He states that the

positive bias in the mean wind speed due to wind-direction fluctuations is much larger than the overspeeding and can be as much as 18%. The ultrasonic anemometer on top of the mast is used to measure the "reference wind speed U_{10}". The less accurate, but also less expensive cup anemometers are used to provide information about the wind-speed profile. The data are gathered on a 1-minute basis.

2.3. Rain

The rain-gauge installation is illustrated in Fig. 3c and Fig. 6. A self-siphoning capacitance rain gauge [17] was installed. It has a number of advantages over a tipping-bucket rain gauge. It allows a continuous measurement at a high resolution (0.02 mm) and as a result it can measure the duration of the rain. A capacitance rain gauge provides a signal representing the rainfall catch whenever requested, while a tipping-bucket rain gauge only gives a signal of the catch after a time when the bucket is full, i.e. typically when 0.1 or 0.2 mm rainfall has been collected. The capacitance rain gauge was placed inside a cylindrical tube that was partly sealed at the top, with only a small part of the gauge cylinder sticking out of the tube (Fig. 3c and Fig. 6). A splash-preventing mat surrounding this part of the gauge cylinder was placed on top of the tube. A semi-circular turf wall was constructed around the rain gauge to reduce the wind error for south-west wind (Fig. 6). The wind error is considered to be the most important error source in horizontal rainfall measurements (i.e. measurements of rainfall through a horizontal plane, e.g. a traditional rain gauge with a horizontal orifice). It is due to the systematic deformation of the wind-flow pattern near the gauge orifice (and hence of the raindrop movements in this flow pattern) by the presence of the gauge body itself (Fig. 7). When the rain gauge is placed at a certain height above ground (typically between 0.5 and 1.5 m), without any precautions, the undermeasurement error is typically 2 to 10 % [18]. But it is clear that as the wind error increases with wind speed [19], it will be much higher for rain gauges positioned on building roofs and at the top of meteorological masts, as is often done for rain gauges on or near test buildings. Various precautions to limit this error are all based on the same goal: to make the air flow horizontal above the gauge orifice (e.g. [18, 20, 21]). One of these precautions is the construction of a (semi-) circular turf wall around the gauge as specified in Fig. 6. It is noted that the rain gauge, just as the meteorological mast, was placed outside the wind-flow pattern that is disturbed by the building for south-west wind (Fig. 4). Horizontal rainfall data are gathered on a 1-minute basis.

2.4. Wind-driven rain

During the year 2000, twenty-three new WDR gauges have been manufactured. At that time, the guidelines for the design of WDR gauges [12] were not yet available. Instead, the results of the gauge-comparison study by Högberg et al. [11] were taken into account by constructing the gauges from PMMA (polymethyl-methacrylate) and by limiting their collection area to 0.2x0.2 m² (Fig. 8). Fig. 1 illustrates the positions and the numbers of the WDR gauges. A large number of gauges were spread across the facade to obtain high-resolution spatial information about the variation of the WDR exposure. Note that the term "high-resolution" is a relative one. It is used here because the number of gauges in this set-up is much higher than in most previous WDR studies. Note that Fig. 3a-b shows that a number of test walls in the sloped-roof module were constructed with their outer surface out of the original facade surface (protruded walls). The same goes for one of the walls in the flat-roof module. The gauges 1-9 are all located on the edges of the protruding white (stucco) facades. The gauges 13-15 are positioned on the protruding facade of the flat-roof module. It is noted that the surface of the latter facade is situated 0.02 m more to the front than the other facades of the flat-roof module. Because we define roof-overhang length in this paper (Fig. 1) as the horizontal distance between the facade surface and the roof gutter, this difference is treated as a local reduction of the roof-overhang length (as indicated in Fig. 1). It will be shown in section 3 that such a small difference in "overhang length" can have a significant influence on the WDR exposure of the facade. The installation of the WDR gauges and their reservoirs is illustrated in Fig. 9. The reservoirs of gauges 1-18 and 22-24 are positioned at the interior of the building. The rainwater that impinges on the collection area (Figs. 9a-b) is deviated through the facade into the inside reservoirs (Fig. 9c), the content of which is measured on a regular basis. A number of reservoirs are equipped with a pressure sensor that measures the height of the water level (Fig. 9d). The most important reasons for mounting the reservoirs inside are: (1) the risk of frost damage to the reservoirs; (2) the sensitivity of the pressure sensors to temperature changes; (3) the reduction of the WDR measurement error by keeping the draining tube as short as possible, by measuring the constant evaporation rate of water from the reservoir and correcting the measurements for this error and by limiting the wind error that would be due to positioning the reservoirs on the outer surface of the facade [12]. It is noted that pressure

sensors were preferred over a tipping-bucket mechanism for two reasons: (1) they allow continuous measurements at a high resolution and (2) the cost: a tipping-bucket rain gauge (500-1000 €) is about 2 to 4 times as expensive as a pressure sensor (280 €). A drawback however of using pressure sensors is the disturbance of the signal caused by the impact of drops that fall from the end of the draining tube on the water surface in the reservoir. The reservoirs of gauges 19 and 20, placed at the top of the terrace module facade, are situated outside the building (Fig. 9e). It was not possible to lead the draining tube to the inside here. The content of the reservoirs that are equipped with pressure sensors is measured on a 1-minute basis. The content of the other reservoirs is measured on a daily basis.

3. Experimental data

3.1. The approach-flow wind-speed profile

As discussed in subsection 2.2, the approach-flow profile of the mean horizontal wind speed is measured at a distance of 20 m upstream of the south-west building facade at four positions on a meteorological mast (at 2 m, 4 m and 6 m height by cup anemometers and at 10 m height by an ultrasonic anemometer). The corresponding mean streamwise horizontal wind-speed values will be denoted by U_2, U_4, U_6 and U_{10}. Below, the procedure that was followed to obtain a power-law wind-speed profile from the measurements is outlined. It is recognized that in reality the wind-speed profile is part of an internal boundary layer and that fitting a power-law is a simplification of reality based on measurements at four positions.

1. Given the complexity of the site, the approach-flow profile will be different for different wind directions. The experimental WDR database focuses on south-west wind direction (225° from north). Therefore, only the data (10-minute average values of wind speed) corresponding to wind directions in the interval [202.5°, 247.5°] were selected.
2. The magnitude of the measured wind speed is highly variable. To be able to perform a statistical analysis on the measured profiles, each "10-minute-measured profile" must be scaled by a reference wind speed. The value measured by the ultrasonic anemometer, U_{10}, was selected as reference wind speed. It is considered to be far more accurate than the cup-anemometer measurements, which can suffer from significant errors as discussed in subsection 2.2. For each 10-minute interval, the values U_2, U_4 and U_6 were divided by U_{10}.
3. Next, the mean value and the standard deviation of the scaled values U_2/U_{10}, U_4/U_{10} and U_6/U_{10} were determined. Based on this information, the parameter α_P (exponent of the power law) was determined using the Markov estimation method [22]. It comprises the use of a weighting technique that incorporates the standard deviations (information on the measurement accuracy) and allows to relatively weigh the different measurements. Note that the standard deviation of U_{10}, given the scaling procedure described in the previous step, is zero. This means that the fitted power law is forced to include this value. An exponent $\alpha_P = 0.176$ has been found. The results (average values, standard deviations and the power-law fit) are given in Fig. 10.

3.2. Accuracy, reliability and selection of wind-driven rain data

The possible errors associated with WDR measurements are [12]: (1) evaporation of adhesion water from the collection area (and from the inner side of the draining tube), (2) evaporative losses from the reservoir, (3) splashing of drops from the collection area, (4) condensation on the collection area and (5) wind errors. The adhesion-water-evaporation error, which is generally considered to be most important [12], is briefly explained. During and after a WDR event, there is always an amount of water (individual drops or water film) adhered to the collection plate. This amount is not collected in the reservoir and hence not measured. After and to a lesser extent also during rain, this *adhesion water* evaporates and an error is generated. In a recent publication concerning the accuracy of WDR measurements on buildings, it is shown that, depending on the type of the gauge and the rain event, this error can be very important [12]. To limit this error and the other errors that can be associated with WDR measurements, a number of guidelines for the selection of accurate and reliable WDR data from experimental WDR databases were proposed [12]. The guidelines are very strict. They are repeated here:

1. Select rain events with large WDR amounts, hence reducing the relative adhesion-water-evaporation error e_{AW} (the adhesion-water-evaporation error is especially important for WDR events with small WDR amounts). This error should be estimated. This can be done by assuming

a worst-case scenario; meaning complete adhesion-water evaporation directly after each interruption of the rainfall (by a dry period) in the rain event [12].
2. Measure the evaporation from the reservoir and correct the measurements for this error.
3. Select rain events for which splashing errors will be absent or small; i.e. rain events characterized by reference wind-speed values U_{10} lower than 10 m/s and with horizontal rainfall intensities with a low probability for large drops: $R_h < 20$ mm/h (Best [23]).
4. Select rain events for which the wind direction during rain is approximately perpendicular to the facade under study, hence limiting the wind error.

Strictly following these guidelines implies that a large amount of the WDR measurement data that are gathered can not be used and that measurements for a long period will be needed to obtain at least a significant number of reliable and useful WDR measurements. It is stressed that the strict character of these guidelines is justified because there are currently no other ways to ensure that the gathered data is accurate. It was chosen to provide only those samples from the experimental WDR database in this paper and on the website that are guaranteed to be accurate and reliable and that are therefore suitable for model development and model validation.

3.3. Selected experimental data

3.3.1. Cumuliform versus stratiform rain events

A distinction is made between cumuliform and stratiform rain events. This terminology stems from the type of clouds generating the rain. *Cumuliform clouds* or heap clouds develop in an unstable atmosphere as a result of fast and local rising air currents. These clouds are isolated and develop vertically. Due to the initially large rate of water-vapor condensation, the rainfall rate from these clouds cannot balance the condensation rate. As a result, the water first accumulates in the cloud to suddenly start precipitating with relatively large intensity. This type of rainfall is referred to as showers. Showers usually start and stop suddenly and are generally of short duration. *Stratiform clouds* or layer clouds develop in a stable atmosphere as a result of widespread cooling and by condensation processes that are slow but persistent. These clouds have wide horizontal dimensions with limited vertical depth. The rainfall rate from these clouds is generally in balance with the rate at which the water vapor condenses. As a result, the precipitation starts and stops slowly, is quite steady (although it can exhibit breaks), often lasts for many hours and is generally of low intensity. Experimental data are provided for both types of rain events.

3.3.2. Experimental data for a cumuliform rain event

The meteorological data record of reference wind speed, reference wind direction and reference horizontal rainfall intensity in the period from 02 to 05/02/2002 is shown in Fig. 11a. The rainfall is of the showery type and of light to moderate intensity. The total horizontal rain amount at the end of the rain event S_h = 15.7 mm. The wind speed is fluctuating between 0 and 8 m/s and the wind direction during rain is approximately south-west (225°, i.e. perpendicular to the south-west facade). Fig. 11b illustrates the temporal distribution of WDR (S_{wdr})[1] at gauge position 13 on the south-west facade. In the beginning of the rain event, no WDR is registered because there is very little rainfall, because the roof overhang effectively shelters the gauge at low wind speed and because the small amount of rain water that reaches the gauge will first be present as adhesion water (it does not run off into the reservoir yet and is hence not yet measured). As the wind speed and the horizontal rainfall intensity increase, the co-occurrence of wind and rain gives rise to high WDR amounts. In a recent publication on the accuracy of WDR measurements on buildings [12], it was shown that for the meteorological conditions in this type of rain events, the error on the WDR measurements is dominated by adhesion-water evaporation. An estimate of this error can be obtained by assuming a worst-case scenario; where all adhesion water evaporates at each interruption of the rain by a dry period. The typical amount of adhesion water that is present at the surface of the WDR gauges used in this study was measured [12]: 0.10 mm. For this rain event, with 8 interruptions of the rainfall by dry periods, the adhesion-water error estimate for the total WDR amount at the end of the rain event is given by: E_{AW} = 8 x 0.1 mm = 0.8 mm. Fig. 11c shows the variation of the ratio of the total WDR amount S_{wdr} to the total horizontal rainfall amount S_h (= 15.7 mm) across the facade at the end of the rain

[1] The collected amount of WDR, "S_{wdr}", is obtained by dividing the volume of water collected by the WDR gauge (in L) by the collection area of the gauge (0.2x0.2 m²). The units of S_{wdr} are thus L/m² or mm (on a vertical surface), similar to the units of horizontal rainfall S_h on a horizontal surface.

event. An error estimate for the ratio S_{wdr}/S_h is obtained by dividing E_{AW} by S_h: ε_{AW} = 0.8 / 15.7 mm = 0.05. The following observations are made:

1. The highest values are found at the top edge of the terrace module (no roof overhang – gauges 19-20).
2. For the flat-roof module: The flat-roof module clearly catches more WDR than the sloped-roof module, which is due to the wind-blocking effect [10] – which is larger for the sloped-roof module – and to the difference in roof overhang length. According to the typical wetting pattern of building facades, the WDR amount is expected to increase from bottom to top and from the middle to the vertical edges of the facade [1]. Despite the presence of the roof overhang, the increase from bottom to top is clear, although it would have been more pronounced without the roof overhang present. Concerning the increase of the values towards the vertical edge of the flat-roof-module facade, it is noted that the values at gauges 13-15 are rather high compared to those at gauges 10-12 and 16-18 (the highest values are expected closest to the vertical edge, i.e. at gauges 16-18, while the values at gauges 13-15 should be in between those at gauges 10-12 and 16-18). This observation is due to the 0.02 m (!) difference in roof overhang for this small part of the facade. This observation has been found systematically for all rain events with wind-speed data of similar or lower magnitude (the wind speed largely determines the effect of the overhang).
3. For the sloped-roof module: The increase of the values from bottom to top of the facade is only present for the gauges 2 and 3, 8 and 9. The gauges near the top of the facade are to some extent sheltered by the roof overhang.

3.3.3. Experimental data for a stratiform rain event

The meteorological data recorded in the period from 25 to 26/02/2002 are shown in Fig. 12a. As opposed to Fig. 11a, the rainfall here is clearly of the *stratiform* type (continuous rainfall lasting for many hours). The horizontal rainfall intensity is light to moderate and the total horizontal rainfall amount S_h = 26.7 mm. Wind speed is situated between 2 and 6 m/s and the wind direction during rain is approximately south-west (225°). Fig. 12b illustrates the temporal distribution of WDR at gauge position 14. During the first 130 minutes of the rain event, no WDR is registered. The roof overhang appears to effectively shelter position 14 during the low wind-speed conditions in the beginning of the rain event. As the wind speed increases and after some delay (gauge collection area first collects adhesion water), WDR is starting to be registered and the WDR catch increases at a more or less constant rate. The adhesion-water evaporation error for the total WDR amount is estimated: E_{AW} = 5 x 0.1 mm = 0.5 mm. Fig. 12c shows the variation of the ratio of the total WDR amount S_{wdr} to the total horizontal rainfall amount S_h (= 26.7 mm) for the rain event across the facade. The error for the ratio S_{wdr}/S_h is $\varepsilon_{AW} = E_{AW}/S_h$ = 0.5 / 26.7 mm = 0.02. The observations are similar to those for the cumuliform rain event:

1. The highest values are found at the top edge of the terrace module.
2. For the flat-roof module: The flat-roof module catches more WDR than the sloped-roof module. The WDR amount increases from bottom to top. Again, the values at gauges 13-15 are rather high compared to those at gauges 10-12 and 16-18 due to the same reason as mentioned above.
3. For the sloped-roof module: The increase of the values from bottom to top of the facade is only present for the lower two gauges (2 and 3, 5 and 6, 8 and 9). The gauges near the top of the facade are to some extent sheltered by roof overhang.

3.3.4. Experimental database

The experimental database can be downloaded from the website of the Laboratory of Building Physics, Katholieke Universiteit Leuven. The website is a part of this paper:

www.kuleuven.be/bwf/projects/WDRdatabase

It contains (for the rain events presented in this paper and for the other selected rain events):

- a detailed description of the building geometry and the surroundings
- the values of the meteorological data record (measurements of reference wind speed, reference wind direction and horizontal rainfall intensity on a 1-minute basis).
- the graphical presentation of the meteorological data record
- the values of the measurements of the WDR amount during and at the end of the rain event

- the graphical presentation of the WDR measurements at the end of the rain event (spatial distribution)
- the adhesion-water error estimates for the WDR measurements

The database only contains six rain events (A to F) that were selected from the total amount of experimental data gathered in the period 09/2001-03/2002. The rain events were selected based on the guidelines provided in subsection 3.2. Rain events with wind direction during rain that is generally perpendicular to the south-west building facade were selected. The results from all selected rain events satisfy the requirements for negligible splashing and have been corrected for evaporation from the reservoir. The remaining important error sources are [12]: adhesion-water evaporation and the wind error. Table 1 provides information about these errors for the six selected rain events: (1) the relative adhesion-water evaporation error $e_{AW} = E_{AW}/S_{wdr}$ for the minimum and maximum total WDR amount collected at a certain position at the end of the rain event (e.g. see Fig. 11c and 12c) and (2) some information concerning the variability and the range of the wind direction that can be seen as a rough indication of the possible wind error. The rain events that were presented in subsection 3.3, A and C, provided the "most accurate" measurement data. The next best rain event is F, although the largest error $e_{AW,max}$ is already very large here. The other rain events, B, D and E generally have higher adhesion-water evaporation errors and a higher variability and wider range of wind direction. Note that rain event D and E show significant deviation of the wind direction from south-west during rain. However, because the wind speed during both rain events is very low (< 3 m/s during rain), the wind error is also expected to be low. Furthermore, the largest deviations in wind direction during rain event D occurs when the wind speed is zero (no WDR). Therefore, both rain events have been included in the database. All other rain events during the period 09/2001-03/2002 provided larger errors or did not satisfy the requirements for data selection mentioned in subsection 3.2. Note that for this particular building, for this (shielded) building site, for this climate and for this type of WDR gauges, 7 months of measurements only provided six valuable rain events.

4. The wind-driven rain coefficient and the wind-driven rain relationship

Experimental data, as provided in this database, can be used for model development and model validation. In this section, the experimental data are used to determine some WDR coefficients, to use them to calculate WDR with the semi-empirical WDR relationship and to briefly address the performance of this relationship.

In the past, the semi-empirical WDR relationship has been the most frequently used tool to calculate the WDR amount on buildings [1]:

$$S_{wdr} = \alpha U_{10} S_h \cos\theta \qquad (1)$$

where S_{wdr} is the WDR amount (mm), α is the WDR coefficient (s/m), U_{10} is the reference wind speed (m/s), S_h is the horizontal rainfall amount (mm) and θ is the angle between the wind direction and the normal to the wall. Note that adding $\cos\theta$ implies that the horizontal streamwise wind-velocity vector with magnitude U_{10} is projected normal to the wall. This relationship is semi-empirical because it is based on a theoretical derivation, while the WDR coefficient is typically obtained based on experimental data [1]. The use of the WDR relationship for calculating WDR on buildings is universally adopted [1]. Also the European Standard Draft PrEN13013-3 [24] for WDR assessment is based on the WDR relationship. Furthermore, a large number of existing HAM (Heat-Air-Moisture) transfer simulation programs employ this relationship to convert the standard meteorological data in the climatic data files (wind speed, wind direction, horizontal rainfall amount) to the corresponding WDR amounts. It is well-known that the WDR coefficient is a pronounced function of the building geometry and of the position on the building facade. On the other hand, the WDR coefficient is often assumed to be independent of wind speed, wind direction and rainfall intensity. As an example, HAM software typically employs constant WDR coefficients.

The generally adopted procedure for WDR assessment with the WDR relationship consists of two stages:

1. *Determining the WDR coefficient*. The WDR coefficient α is typically determined from hourly measurements of wind speed, wind direction, horizontal rainfall and of WDR at a certain position on a building facade. The measured values for WDR, S_{wdr}, are plotted as a function of the product

$U_{10}S_h\cos\theta$ (Fig. 13). The inclination of the straight line through the origin that represents a best fit (least-squares) through the experimental data is taken as the value of the WDR coefficient.

2. *Application of the WDR relationship*. Once the value of the WDR coefficient α has been determined (e.g. for several positions on a building facade), it is used for future WDR assessment with Eq. (1), in which it is considered to be a value that is constant in time. Measured standard meteorological data (generally on an hourly basis) of wind speed, wind direction and horizontal rainfall are used as input in Eq. (1).

The data from all six WDR events (A to F) provided in the database have been used to determine the WDR coefficient on two positions on the south-west building facade (Fig. 13). A significant amount of scatter is present; the correlation is low. The reasons for this are: (1) the WDR coefficient is in reality a function of time, because it depends on wind speed, wind direction and rainfall intensity, (2) the measurement errors are variable in time and (3) WDR measurements can suffer from a significant time lag, i.e. it takes some time before the impinged raindrops have run off into the reservoir (as was also indicated in Fig. 11b and 12b). As a result, the obtained WDR coefficients can only be regarded as rough estimates.

In Fig. 14, these WDR coefficients have been used to calculate the cumulative WDR amounts S_{wdr} based on the hourly experimental data for U, S_h and θ. This was done for the two rain events in Fig. 11a and 12a. Fig. 14 shows that WDR relationship provides quite good estimates of the WDR in these two cases. Here, the discrepancies are due to the actual temporal variability of the coefficient α and the errors in the WDR measurements that were used to determine α. Because both the temporal variability and the measurement errors are larger for the cumuliform rain event, the discrepancies (Fig. 14a versus b) are also larger for this rain event. Fig. 14 might suggest that the WDR relationship is a good tool for WDR assessment. However, note that this exercise is not realistic. In this case, the WDR coefficients were determined from the same rain events for which they were applied. This was done to show the influence of the temporal variability of α and of measurement errors. In reality, the WDR coefficients are determined for different rain events than those for which they will be applied. Furthermore, for all six rain events in the database, the variables wind speed, wind direction and rainfall intensity are situated within a certain (narrow) interval (e.g., wind speed does not exceed 8 m/s, rainfall intensity is always below 14 mm/h). In reality and for less favorable conditions, larger discrepancies are expected. Further research will specifically focus on the performance of the WDR relationship in these cases.

5. Discussion

The building, the building site and the measurement set-up are not perfect. The most important drawback, at least for early validation studies, is the complexity of the surroundings; especially the row of trees that is situated west of the test building. For early validation studies it would be better to avoid the presence of trees at the building site, because modeling trees is quite complex and not well established in Computational Wind Engineering. However, it is a research topic that should be addressed in the future. Nevertheless, the experimental WDR database that is presented in this paper is considered to be a valuable tool for model development and model validation. The reason is that it satisfies the requirements listed in section 1 of this paper: it comprises and/or is accompanied by a detailed description of the building geometry and the building site, a detailed description of the measurement set-up, measurements of the reference wind speed, wind direction and horizontal rainfall intensity in “free-field” conditions, WDR measurements at the facade with a high resolution in space and time and error estimates for the WDR measurements. No other experimental databases that satisfy these requirements are known to the authors. Even experimental databases that satisfy most of these requirements are scarce.

The presence of the trees at the site of the VLIET test building was the reason for measuring the upstream wind-speed profile (south-west wind) downstream of the row of trees and as close as possible to the building facade to obtain a representative description of the approach-flow profile as input for future numerical studies. For the same reason, the horizontal rainfall measurements were conducted at the same location. Furthermore, in the design of the measurement set-up, attention has been paid to positioning the equipment for wind and horizontal rainfall measurements outside the wind-flow pattern that is disturbed by the building and to limiting the wind error that is associated with horizontal-rain measurements by the construction of a semi-circular turf wall around the rain gauge.

Although measurements at the VLIET test site have been conducted for 7 months, only a limited number of rain events (six) are considered to be suitable for WDR studies. Guidelines for the selection of accurate and reliable WDR data from experimental databases were provided. These guidelines are strict and should be strictly adhered to, because no other information is currently available to guarantee

accurate and reliable WDR data. Following these guidelines implies that a large part of the WDR measurements cannot be used and that only a few rain events are obtained that are accurate and reliable. One of these guidelines is that the wind direction during rain should generally be perpendicular to the facade and hence to the collection area of the WDR gauges, to make sure that the wind error in the WDR measurements is limited. For other wind directions, this error can become important. This is one of the reasons why the focus in this paper has only been on south-west wind. The other reason is the complexity and the proximity of the surroundings for the other wind directions.

6. Conclusions

With the specific intention to provide experimental wind-driven rain (WDR) data for model development and model validation, a new measurement set-up for wind, rain and WDR has been designed and installed at the Laboratory of Building Physics (Katholieke Universiteit Leuven). This paper has provided a description of the building, the building site and the measurement set-up, as well as a few samples of the experimental WDR database, including a link to a website from which the experimental WDR database can be downloaded. The database has been carefully selected by adhering to strict guidelines for accuracy and reliability. The authors hope that it will serve as a tool for model development and model validation in WDR studies, for semi-empirical models but especially for CFD-based WDR models.

Acknowledgements

The first author is currently a post-doctoral research fellow of the FWO-Flanders. The FWO-Flanders (Research Fund - Flanders) supports and stimulates fundamental research in Flanders. Their contribution is gratefully acknowledged. The construction of the wind-driven rain measurement set-up that has been described in this paper has been made possible by additional financial support of the FWO-Flanders (FWO Krediet aan Navorsers), for which we are very grateful. We would like to thank our colleague Peter Moonen for constructing the website associated with this paper. Special thanks are also due to the anonymous reviewers for thoroughly reading the manuscript and for valuable suggestions.

Nomenclature

E_{AW}	absolute adhesion-water-evaporation error (mm)
e_{AW}	relative adhesion-water-evaporation error ($e_{AW} = E_{AW}/S_{wdr}$) (-)
k	turbulent kinetic energy (m^2/s^2)
R_h	horizontal rainfall intensity (mm/h)
S_h	horizontal rainfall amount (mm)
S_{wdr}	wind-driven rain amount (mm)
U_2, U_4, U_6, U_{10}	reference wind speed at 2, 4, 6, 10 m height (m/s)
U, V, W	streamwise, vertical and lateral component of mean wind-velocity vector (m/s)
x, y, z	Cartesian co-ordinates (x = streamwise, y = vertical, z = lateral co-ordinate) (m)
y_0	aerodynamic roughness length (m)
Z	resultant horizontal wind-velocity vector (m/s)
α	wind-driven rain coefficient (s/m)
α_P	power-law exponent (-)
ε_{AW}	adhesion-water-evaporation error for the ratio S_{wdr}/S_h ($\varepsilon_{AW} \approx E_{AW}/S_h$) (-)
ε	turbulence dissipation rate (m^2/s^3)
θ	angle between wind direction and normal to the wall (°)
φ	wind direction (° from north)
IBL	Internal Boundary Layer
HAM	Heat-Air-Moisture
HAMTIE	Heat-Air-Moisture Transfer in highly Insulated building Envelope parts
RANS	Reynolds-Averaged Navier-Stokes equations
VLIET	Vlaams ImpulsProgramma voor EnergieTechnologie
WDR	Wind-Driven Rain

References

[1] B. Blocken, J. Carmeliet, A review of wind-driven rain research in building science. J. Wind Eng. Ind. Aerodyn. 92, 13 (2004) 1079-1130.

[2] E.C.C. Choi, Numerical simulation of wind-driven rain falling onto a 2-D building, Asia Pacific Conf. on Computational Mechanics, Hong Kong, 1991, pp. 1721-1728.

[3] E.C.C. Choi, Simulation of wind-driven rain around a building, J. Wind Eng. Ind. Aerodyn. 46&47 (1993) 721-729.

[4] E.C.C. Choi, Determination of wind-driven rain intensity on building faces, J. Wind Eng. Ind. Aerodyn. 51 (1994) 55-69.

[5] Karagiozis, A., Hadjisophocleous, G., Cao, S. Wind-driven rain distributions on two buildings. J. Wind Eng. Ind. Aerodyn. 67&68 (1997) 559-572.

[6] Hangan, H, Wind-driven rain studies. A C-FD-E approach, J. Wind Eng. Ind. Aerodyn. 81 (1999) 323-331.

[7] B. Blocken, J. Carmeliet, Spatial and temporal distribution of driving rain on a low-rise building, Wind Struct. 5, 5 (2002) 441-462.

[8] F.J.R. van Mook, Driving rain on building envelopes, Ph.D. thesis, Building Physics Group (FAGO), Eindhoven University of Technology, Eindhoven University Press, Eindhoven, The Netherlands, 2002, 198 p.

[9] D. Segersson, Numerical quantification of driving rain on buildings, Reports Meteorology and Climatology, No. 103, Swedish Meteorological and Hydrological Institute (SMHI), 2003.

[10] B. Blocken, J. Carmeliet, The influence of the wind-blocking effect by a building on its wind-driven rain exposure, J. Wind Eng. Ind. Aerodyn. (2005). Revised version submitted.

[11] A.B. Högberg, M.K. Kragh, F.J.R. van Mook, A comparison of driving rain measurements with different gauges, Proceedings of the 5th Symposium of Building Physics in the Nordic Countries, Gothenburg, 1999, pp. 361-368.

[12] B. Blocken, J. Carmeliet, On the accuracy of wind-driven rain measurements on buildings, Build. Environ. (2005) In press.

[13] H. Hens, Applied Building Physics 1, Boundary conditions and performance requirements (In Dutch; Toegepaste Bouwyfsica 1, Randvoorwaarden en prestatie-eisen), Third Edition, Acco, Leuven, 1996.

[14] T-H. Shih, W.W. Liou, A. Shabbir, J. Zhu, A new k-ε eddy-viscosity model for high Reynolds number turbulent flows – model development and validation, Comp. Fluids 24, 3 (1995) 227-238.

[15] B.E. Launder, D.B. Spalding, The numerical computation of turbulent flows, Comput. Method. Appl. M. 3 (1974) 269-289.

[16] L. Kristensen, The cup anemometer – and other exciting instruments, Doctor Technices Thesis, Risø National Laboratory, Technical University of Denmark, 1993.

[17] N.A. Nystuen, J.R. Proni, P.G. Black, J.C. Wilkerson, A comparison of automatic rain gauges, J. Atmos. Ocean. Tech. 16 (1996) 62-73.

[18] WMO, World Meteorological Organization, Guide to meteorological instruments and methods of observation, Sixth edition, WMO-No. 8, 1996.

[19] WMO, World Meteorological Organization, Methods of correction for systematic error in point precipitation measurement for operational use (Sevruk B.), Operational Hydrology Report, WMO-No. 589, Geneva, 1982.

[20] Meteorological Office, Handbook of meteorological instruments, Part 1. Instruments for surface observations, Her Majesty's Stationary Office, London, 1956, 458 p.

[21] G. Sumner, Precipitation: process and analysis. John Wiley & Sons, 1988, 444 p.

[22] J.V. Beck, K.J. Arnold, Parameter estimation in engineering and science. Wiley, New York, 1977.

[23] A.C. Best, The size distribution of raindrops, Q. J. Roy. Meteor. Soc. 76 (1950) 16-36.

[24] CEN. Hygrothermal performance of buildings – Climatic data – Part 3: Calculation of a driving rain index for vertical surfaces from hourly wind and rain data. Draft prEN 13013-3, 1997.

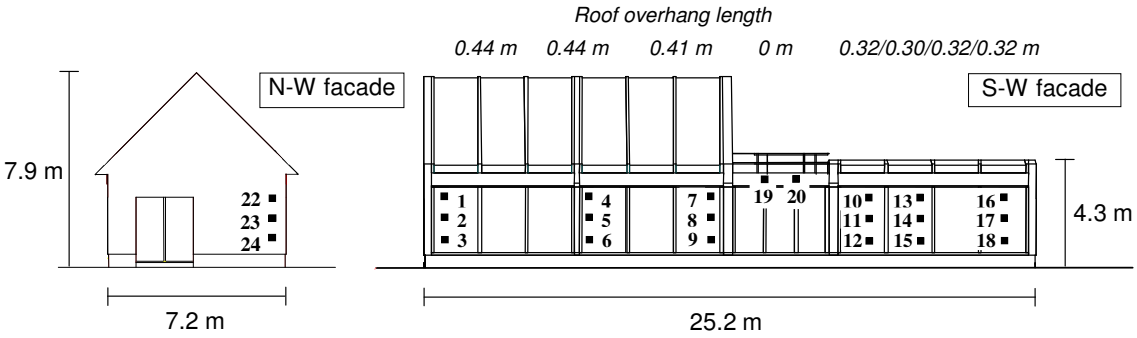

Fig. 1 VLIET test building. North-west and south-west facade. The building dimensions, including roof overhang length, and the positions and numbers of the wind-driven rain gauges (indicated by black squares) are indicated.

Fig. 2 View at the terrain south-west of the VLIET building. (Photograph taken with the back against the south-west facade).

Fig. 3 VLIET test building. (a) View from west illustrating the protruding and recessed facade parts and the wind-driven rain gauges on the facade. (b) View from south. (c) Capacitance rain gauge placed in a sealed tube and surrounded by a semi-circular turf wall. (d) Meteorological mast equipped with 3 cup anemometers positioned at 2, 4 and 6 m height above ground and with an ultrasonic anemometer positioned at 10 m height above ground. The mast is situated at a distance of 20 m in front of the south-west facade. (e) Detail of the ultrasonic anemometer on top of the mast.

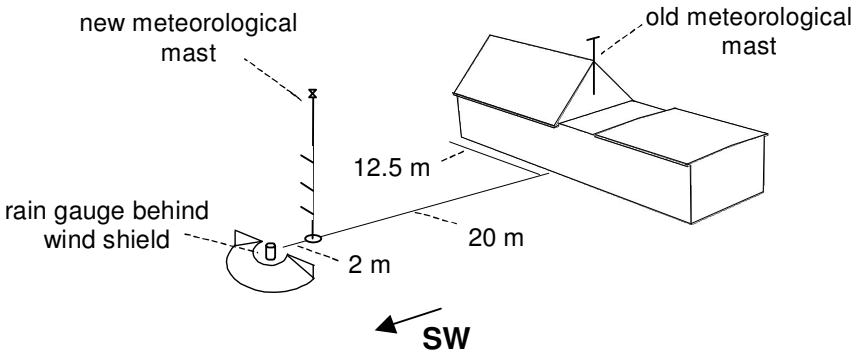

Fig. 4 Location of the old meteorological mast on top of the building roof and location of the new meteorological station (mast and horizontal rain gauge) in front of the south-west facade.

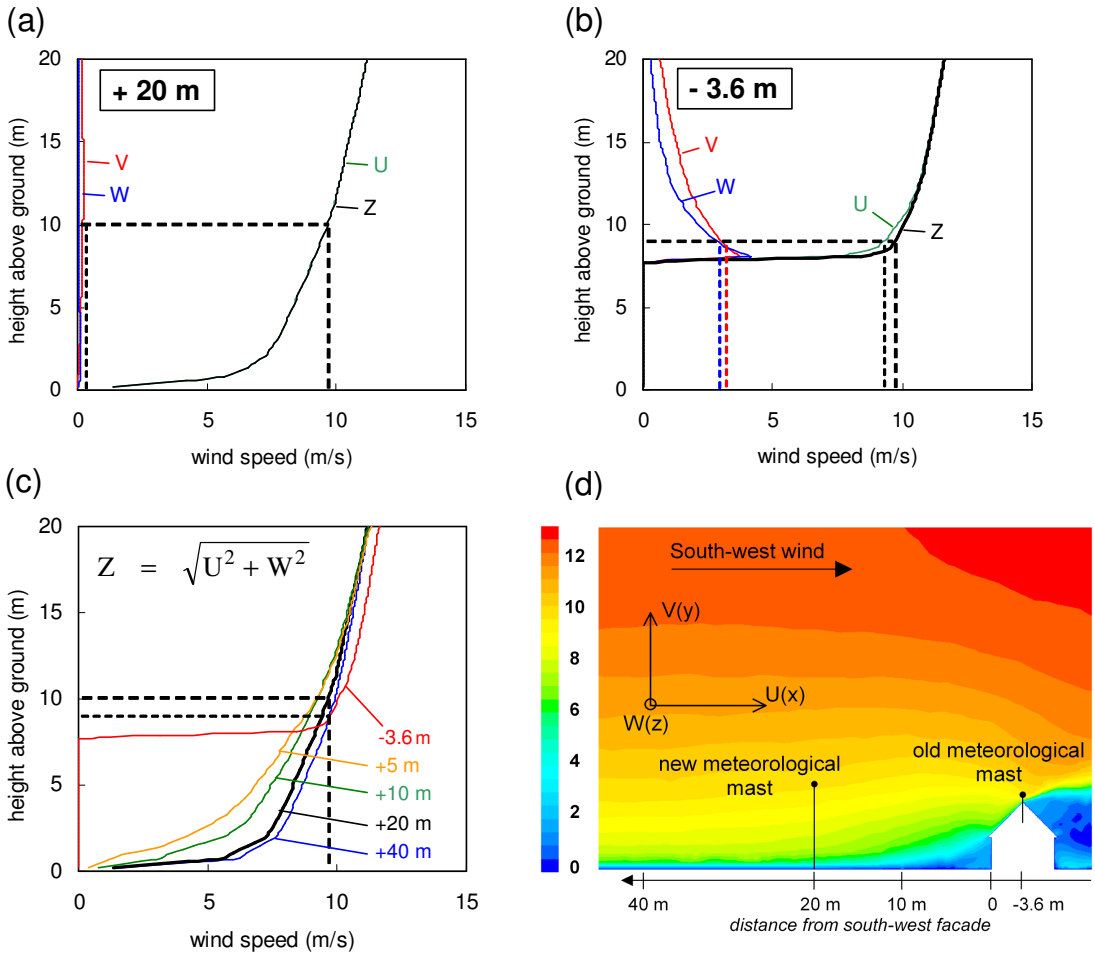

Fig. 5 CFD-simulation results to determine the "optimal" location of the meteorological mast in front of the south-west facade. The axis conventions are given in Fig. 5d, as well as an axis indicating the distance from the south-west facade. (a) Vertical wind-speed profiles (x-, y-, z-components U, V, W and the resultant horizontal component Z) at 20 m in front of the south-west facade and (b) at the location of the old mast on top of the building roof. (c) Vertical profiles of the resultant horizontal wind speed Z at various positions from the south-west facade. (d) Contour plot of the resultant horizontal wind speed Z in a vertical plane that is perpendicular to the building facade (contours are given in m/s; reference wind speed of inlet profile in CFD simulation U_{10} = 10 m/s).

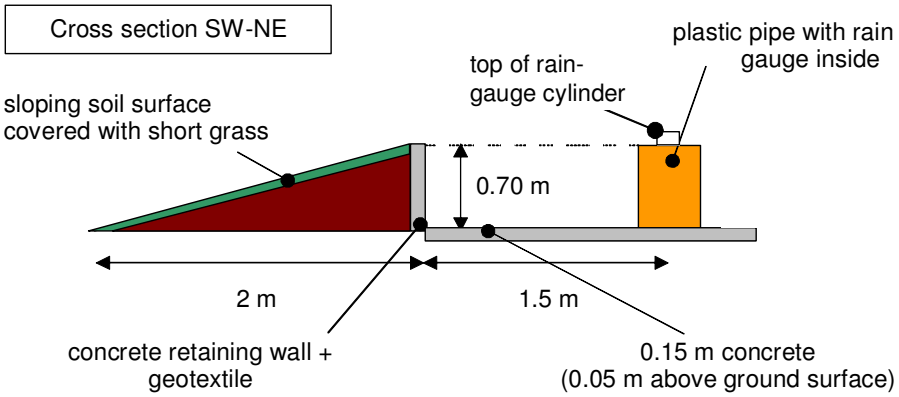

Fig. 6 Design of the measurement set-up for horizontal rainfall. Cross-section (south-west – north-east) of the rain-gauge tube and the semi-circular turf wall.

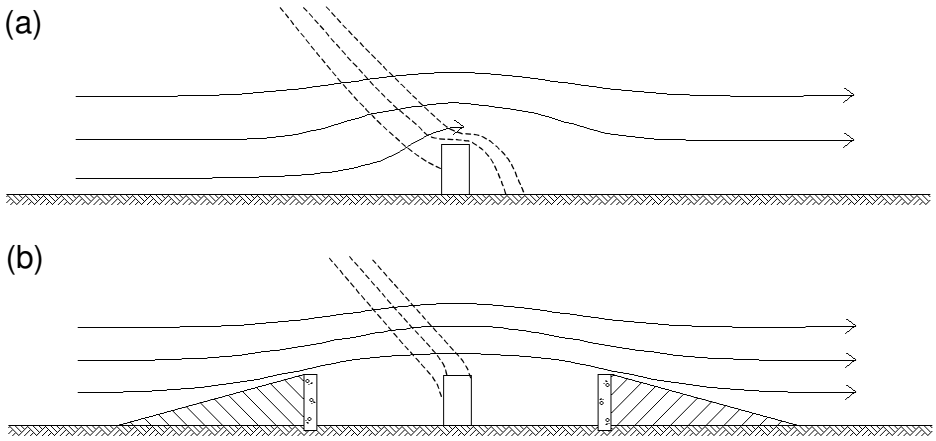

Fig. 7 (a) Cross-section of a rain gauge exposed to wind. The gauge body disturbs the wind-flow pattern and the raindrops (trajectories are displayed with dashed lines) are swept over the rim of the gauge due to the sudden increase in vertical wind speed at this location. This introduces the so-called “wind error”. (b) Cross-section of a rain gauge sheltered from wind by a circular turf wall around it. The wind velocity over the orifice of the rain gauge is approximately horizontal and as a result the trajectories of the drops are not (or only slightly) deflected, which prevents (or at least strongly reduces) the wind error.

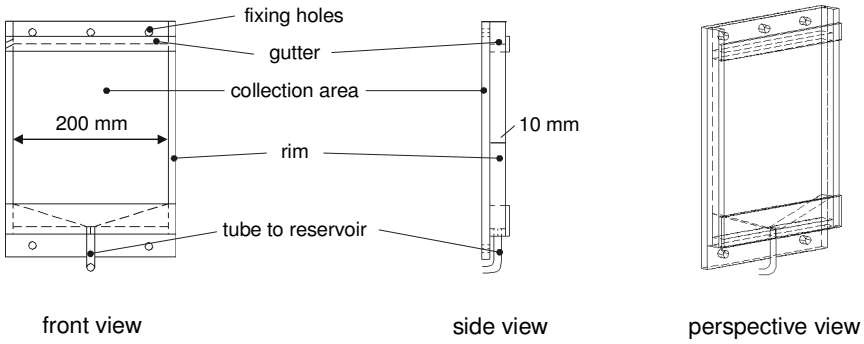

Fig. 8 Wind-driven rain gauge designed, manufactured and installed at the Laboratory of Building Physics, Katholieke Universiteit Leuven. The gauge is made of PMMA (polymethyl-methacrylate) with a collection area A = 0.2x0.2 m².

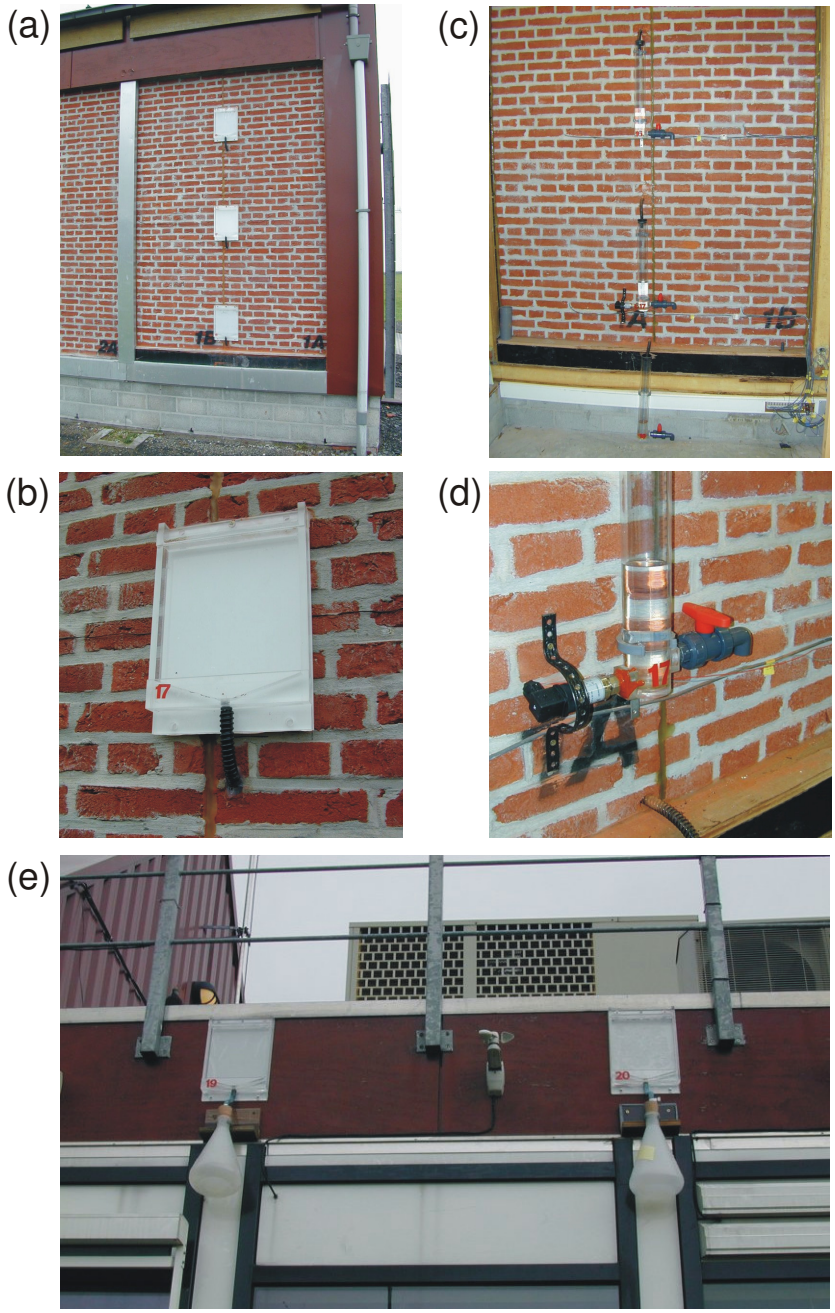

Fig. 9 (a) Wind-driven rain gauges positioned at the facade. (b) Detail of wind-driven rain gauge. (c) The rainwater collected by the gauges is deviated through the facade into the reservoirs fixed at the inside of the building. (d) A number of reservoirs are equipped with a pressure sensor to measure the height of the water level in the reservoirs. (e) Two gauges are positioned at the top of the terrace-module facade. Their reservoirs are situated outside because it was not possible to lead the draining tube through the facade at this location.

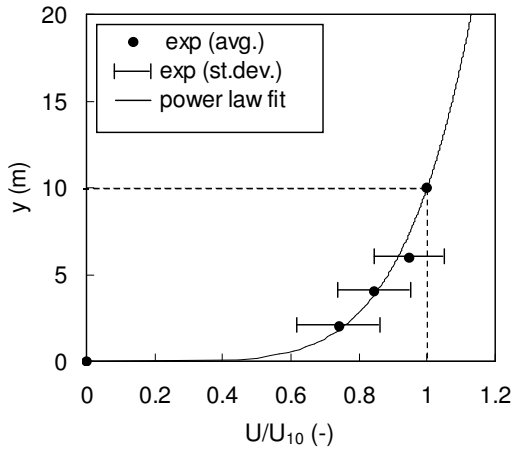

Fig. 10 Presentation of scaled wind speed U/U_{10}: measurements (average values (dots) and standard deviations (bars) at 2 m, 4 m, 6 m and 10 m height) and a power-law fit with power-law exponent $\alpha_P = 0.176$.

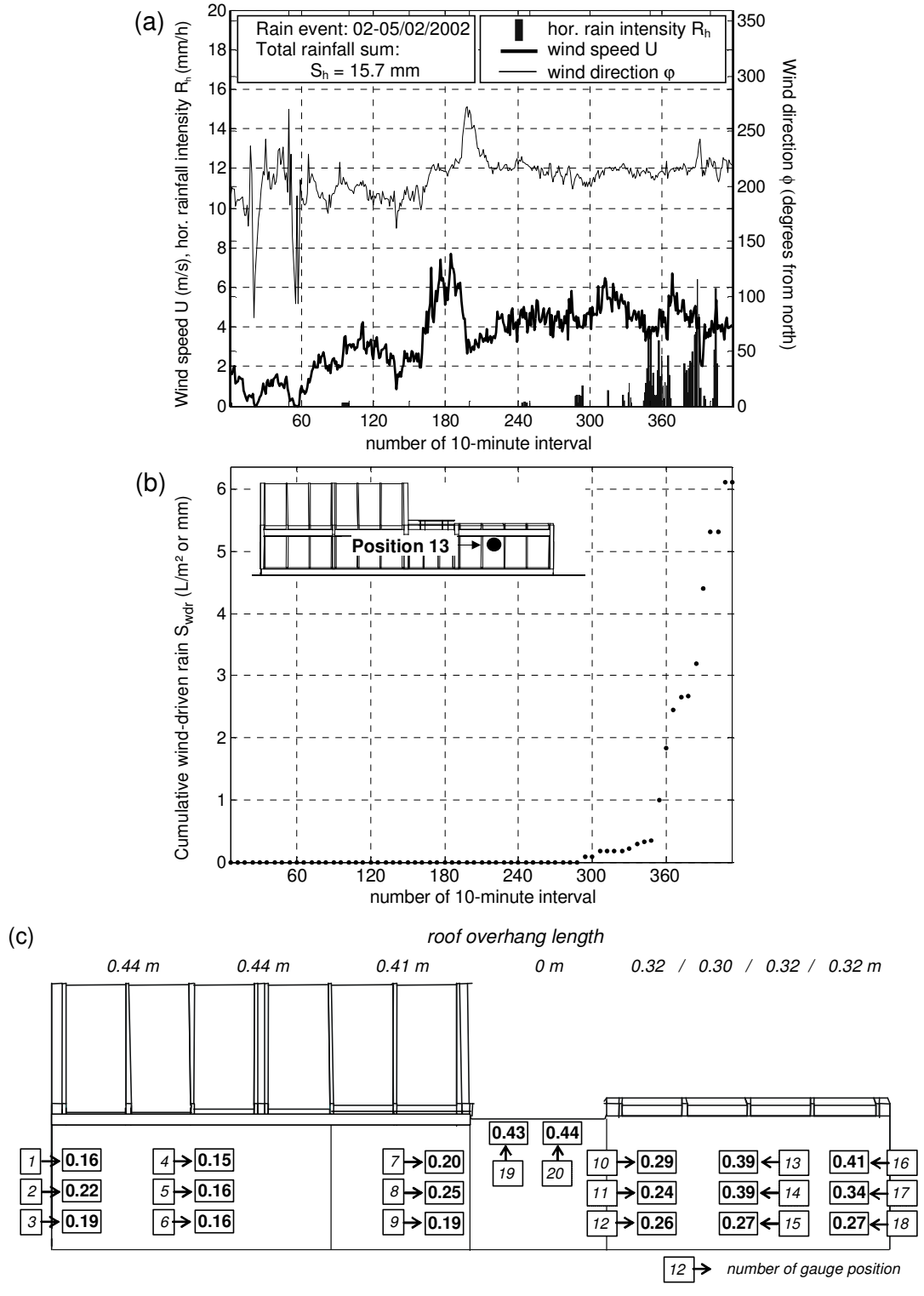

Fig. 11 Measurement results for a cumuliform rain event. (a) Horizontal rainfall intensity, wind speed and wind direction measured during the rain event (and averaged on a 10-minute basis). Total rainfall amount S_h = 15.7 mm. (b) Temporal distribution of the cumulative wind-driven rain amount S_{wdr} during the rain event at position 13. (c) Spatial distribution of the ratio S_{wdr}/S_h (total wind-driven rain amount to total horizontal rainfall amount) for the rain event.

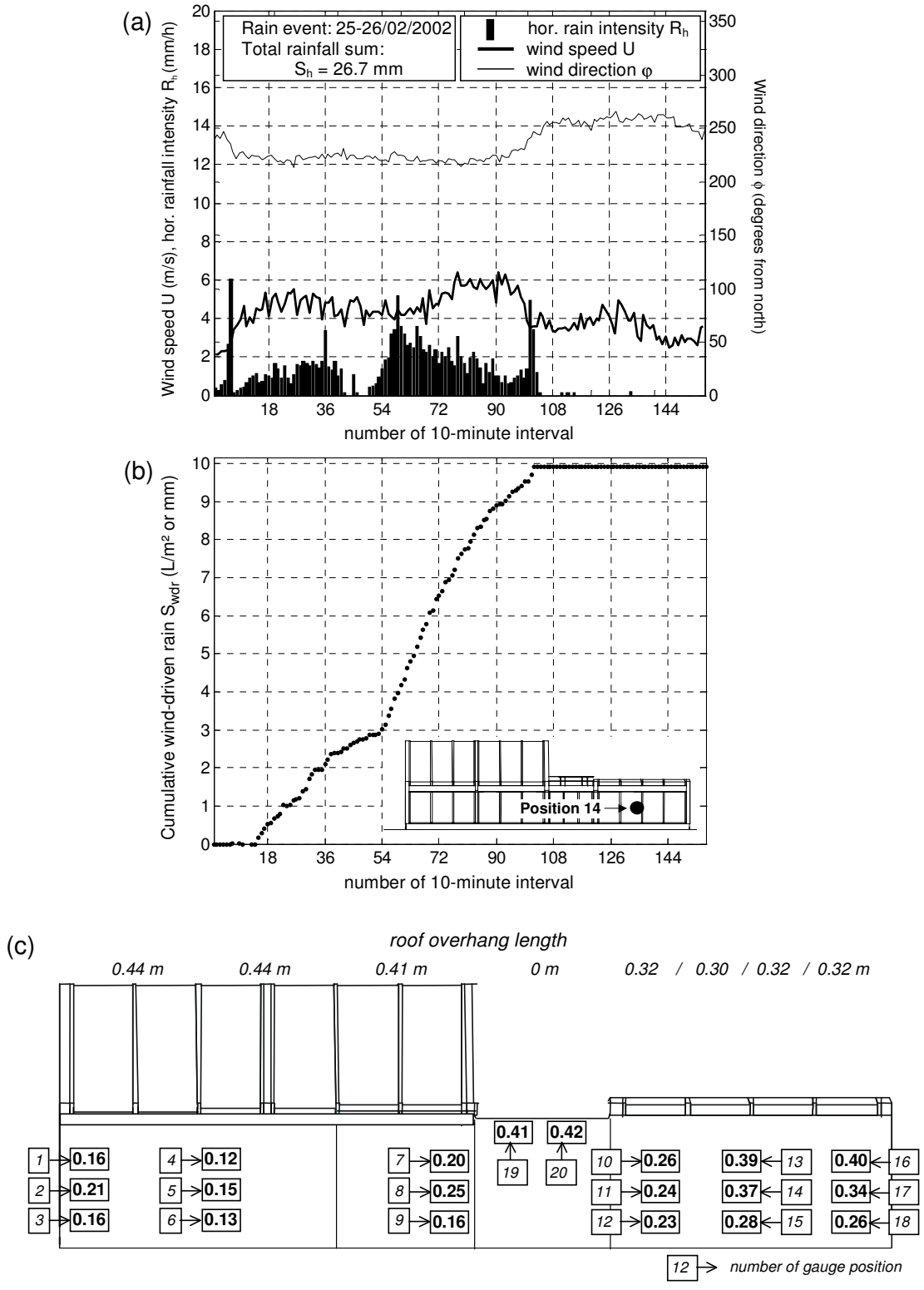

Fig. 12 Measurement results for a stratiform rain event. (a) Horizontal rainfall intensity, wind speed and wind direction measured during the rain event (and averaged on a 10-minute basis). Total rainfall amount S_h = 26.7 mm. (b) Temporal distribution of the cumulative wind-driven rain amount S_{wdr} during the rain event at position 14. (c) Spatial distribution of the ratio S_{wdr}/S_h (total wind-driven rain amount to total horizontal rainfall amount) for the rain event.

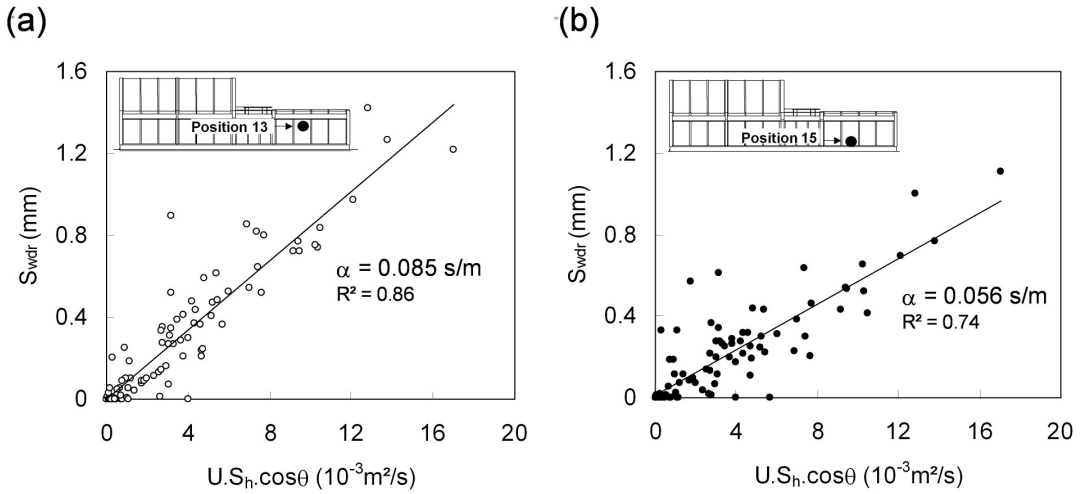

Fig. 13. Determination of the wind-driven rain coefficient at two positions on the south-west facade by a least-squares fit through hourly experimental data.

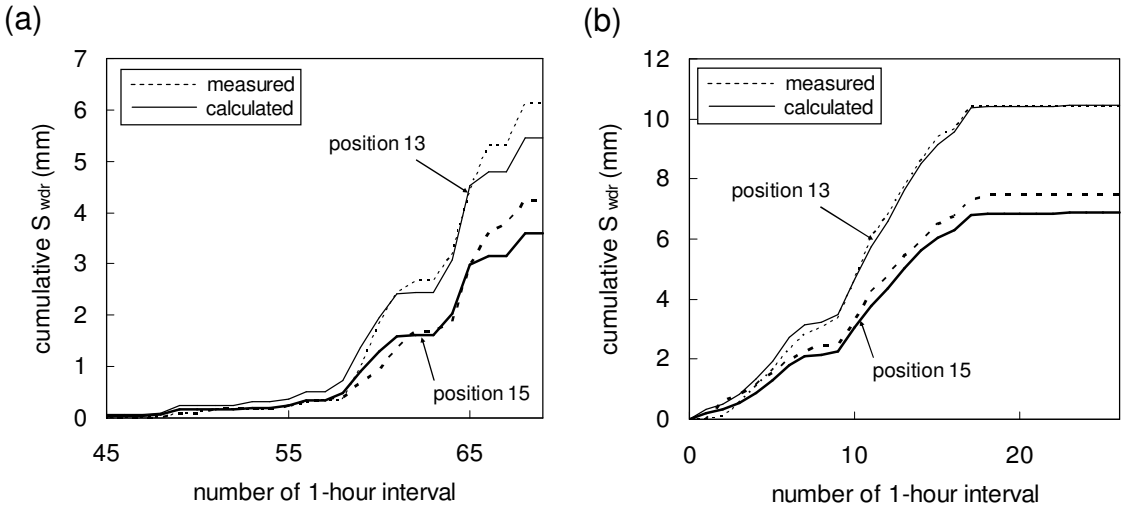

Fig. 14. Comparison between the cumulative calculated and measured WDR amount during (a) the rain event in Fig. 11a and (b) the rain event in Fig. 12a, for two positions at the south-west building facade.

Table 1. Maximum and minimum relative adhesion-water evaporation errors $e_{AW,max}$ and $e_{AW,min}$ for the minimum and maximum ratios S_{wdr}/S_h at the end of the rain event, respectively. Indication of the variability and the range of the wind direction φ.

Rain event	ε_{AW} ([a])	$(S_{wdr}/S_h)_{min}$	$(S_{wdr}/S_h)_{max}$	$e_{AW,max}$	$e_{AW,min}$	φ variability ([b])	φ-range
A	0.05	0.15	0.44	0.33	0.11	constant	225°
B	0.04	0.03	0.29	1.33	0.14	moderate	200°-275°
C	0.02	0.12	0.42	0.17	0.05	almost constant	225°-250°
D	0.05	0	0.12	-	0.42	very high ([c])	([c])
E	0.02	0.01	0.17	2.00	0.12	high	150°-215°
F	0.05	0.06	0.36	0.83	0.14	constant	225°

([a]) Ratio of error E_{AW} to the total horizontal rainfall amount S_h. It is an estimate of the absolute error for the ratio S_{wdr}/S_h

([b]) Indication of the variability of the wind direction φ during rain

([c]) Variability is very high (no clear range of wind directions) during rain but this happens at those moments when the wind speed is nearly zero (no WDR).